

An Investigation of the Mechanical Properties of Some Martian Regolith Simulants with Respect to the Surface Properties at the InSight Mission Landing Site

Pierre Delage¹ · Foivos Karakostas² · Amine Dhemaied¹ · Malik Belmokhtar¹ · Philippe Lognonné² · Matt Golombek³ · Emmanuel De Laure¹ · Ken Hurst³ · Jean-Claude Dupla¹ · Sharon Kedar³ · Yu Jun Cui¹ · Bruce Banerdt³

Received: 18 July 2016 / Accepted: 31 January 2017 / Published online: 15 February 2017
© Springer Science+Business Media Dordrecht 2017

Abstract In support of the InSight mission in which two instruments (the SEIS seismometer and the HP³ heat flow probe) will interact directly with the regolith on the surface of Mars, a series of mechanical tests were conducted on three different regolith simulants to better understand the observations of the physical and mechanical parameters that will be derived from InSight. The mechanical data obtained were also compared to data on terrestrial sands. The density of the regolith strongly influences its mechanical properties, as determined from the data on terrestrial sands. The elastoplastic compression volume changes were investigated through oedometer tests that also provided estimates of possible changes in density with depth. The results of direct shear tests provided values of friction angles that were compared with that of a terrestrial sand, and an extrapolation to lower density provided a friction angle compatible with that estimated from previous observations on the surface of Mars. The importance of the contracting/dilating shear volume changes of sands on the dynamic penetration of the mole was determined, with penetration facilitated by the $\sim 1.3 \text{ Mg/m}^3$ density estimated at the landing site. Seismic velocities, measured by means of piezoelectric bender elements in triaxial specimens submitted to various isotropic confining stresses, show the importance of the confining stress, with lesser influence of density changes under compression. A power law relation of velocity as a function of confining stress with an exponent of 0.3 was identified from the tests, allowing an estimate of the surface seismic velocity of 150 m/s. The effect on the seismic velocity of a 10% proportion of rock in the regolith was also studied. These data will be compared with in situ data measured by InSight after landing.

This article has been updated because during article processing an error occurred in one of the author's names. The author's name "Sharon Kedar" has been corrected in this article and should be regarded as final version by the reader.

✉ P. Delage
pierre.delage@enpc.fr

¹ Ecole des Ponts ParisTech, Laboratoire Navier (CERMES), Paris, France

² Institut de Physique du Globe de Paris-Sorbonne Paris Cité, Université Paris Diderot, Paris, France

³ Jet Propulsion Laboratory, NASA – California Institute of Technology, Pasadena, USA

Keywords Mars · InSight mission · Regolith simulants · Density · Mechanical properties · Seismic velocity · Elastic response

1 Introduction

The InSight mission (Interior Exploration using Seismic Investigations, Geodesy and Heat Transport, Banerdt et al. 2013) is devoted to better understand the interior structure of Mars by using, among other instruments, a seismometer (SEIS, Lognonné et al. 2015; Lognonné and Pike 2015) provided by the French Space Agency (CNES), a heat flow probe to determine the temperature gradient at the surface (HP³, Spohn et al. 2012) provided by the German Space Agency (DLR) and precision tracking. Both instruments will be placed on the Mars surface by the Instrument Deployment Arm (IDA) of the spacecraft. Landing is planned in November 2018. The temperature gradient will be measured by a series of thermometers in the first 5 meters of the surface by a tether attached to a mole that will be dynamically penetrated into the surface layer. Both instruments will interact with a 3–17 m thick regolith at the landing site, produced by impact comminution and eolian activity (Golombek et al. 2016).

To better understand the interactions between these instruments and the regolith, an investigation of the mechanical properties of three regolith simulants was conducted. Although very common in terrestrial geotechnics, dynamic penetration in sands is quite a complex phenomenon involving the shearing properties of sand at large strains, with significant importance of shear induced plastic volume changes through either contraction (for loose sand) or dilation (for dense sand). For the seismometer, the estimation of the elastic properties at the surface on which the device will be placed is another important factor, together with that of the seismic velocities in the regolith for understanding the interior of Mars (see Kedar et al. 2017).

The main parameter affecting the mechanical properties of sand is density, that in turn depends on characteristics including the grain size distribution and the shape and angularity of the grains. As a consequence, the estimation of possible density values at the surface on which the SEIS seismometer will be placed and the 5 meters penetrated by the mole of the HP³ device is an important issue that will be addressed here, based on both existing observations of the properties of the Martian regolith, and on laboratory measurements of the mechanical properties of three different Mars regolith simulants.

2 Background

Many studies and detailed descriptions of the physical properties of the surface materials of Mars have been provided by the interaction of arm scoops and rover wheels from the successful landers (Viking Landers 1 and 2, Phoenix lander) and rovers (Sojourner rover of Mars Pathfinder—MPF, Spirit and Opportunity rovers of Mars Exploration Rovers—MERs, and Curiosity—Mars Science Laboratory). Remote sensing observations from orbiters, including NASA's Viking Orbiters, Mars Global Surveyor, Mars Odyssey, and Mars Reconnaissance Orbiter (MRO) and ESA's Mars Express (MEX) have also contributed to understanding the physical properties of surface materials. A synthesis of the observations of the physical properties of Martian surface materials is provided by Christensen and Moore (1992), Herkenhoff et al. (2008) and Golombek et al. (2008). Various Mars regolith simulants have also been tested in Earth laboratories (e.g. Alshibli et al. 2004; Seiferlin et al. 2008; Peters et al. 2008; Vrettos 2012; Becker and Vrettos 2016).

The regolith on Mars results from impact gardening and other geological processes that have affected the surficial layer. Unlike lunar regolith, the Mars surface layer is also mod-

Table 1 Characteristics of some Martian surface materials (Golombek et al. 2008, Chap. 20)

Surface material	Bulk density (Mg/m ³)	Grain size (mm)	Cohesion (kPa)	Friction angle (°)	Thermal inertia (J m ⁻² K ⁻¹ s ^{-1/2})
Drift	1–1.3	0.001–0.01	0–3	15–21	40–125
Sand	1.1–1.3	0.06–0.2	0–1	30	60–200
Crusty to cloddy sand	1.1–1.6	0.005–0.5	0–4	30–40	200–326
Blocky, indurated soil	1.2–2	0.05–3	3–11	25–33	368–410
Dense float rock, volcanic	2.6–2.8	2–2000	1000–10000	40–60	> 1200–2500
Clastic rock, Columbia Hills	2				620–1100
Sulfate rock, Meridiani	< 2				> 400–1100

Data derived from Moore et al. (1987, 1999), Moore and Jakosky (1989), Christensen and Moore (1992), Arvidson et al. (2004a, 2004b), Christensen et al. (2004a, 2004b), Herkenhoff et al. (2004a, 2004b), Fergason et al. (2006a) and Chap. 20 from Bell.

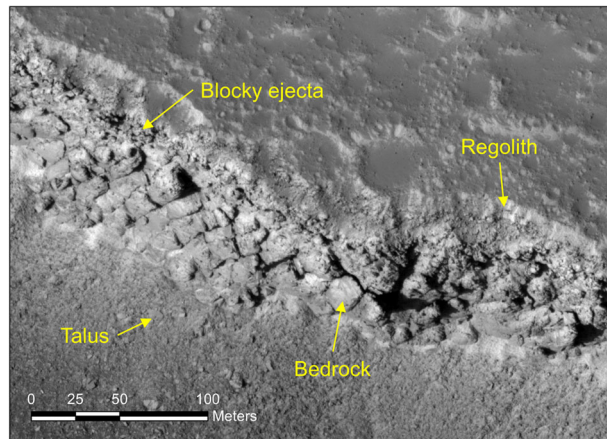
ified by aeolian processes that sort by grain size and produces rounded grains (McGlynn et al. 2011; Goetz et al. 2010). Golombek et al. (2008, 2016) have summarized the physical properties of the regolith on Mars using observations of remote sensing data, comparisons to previous in-situ observations and observations of the InSight landing site.

The main properties of various Martian surface materials taken from a synthesis provided by Golombek et al. (2008) are given in Table 1. Sand deposits comparable to that expected at the InSight landing site, have a bulk density estimated between 1000 and 1300 kg/m³, grain sizes between 0.06 and 0.2 mm, a low cohesion between 0 and 1 kPa and an angle of internal friction around 30°. The table also provides estimates of the thermal inertia of these materials (Piqueux and Christensen 2011), defined as $I = (k\rho c)^{1/2}$, where k is the thermal conductivity, ρ is the bulk density of the surface material, and c is the specific heat. The thermal inertia represents the resistance to a change in temperature of the upper 2–30 cm of the surface. Fine particles change temperature quickly and so have a lower thermal inertia, as observed for the very fine drift material (between 40 and 125 J m⁻² K⁻¹ s^{1/2}). Higher thermal inertia surfaces correspond to larger particles, with values between 60 and 200 J m⁻² K⁻¹ s^{1/2} for sand and higher values for coarser materials. Note that cementation of grains increases the thermal inertia, providing an indication of possible cohesion, which must be less than a few kPa.

More detailed examination of the surface properties at the InSight landing site (Golombek et al. 2016) indicates a moderately low thermal inertia close to 180 J m⁻² K⁻¹ s^{1/2}, which corresponds to cohesionless fine sand 0.170 micron in diameter. Observations of rocky ejecta craters, exposed nearby scarps, and regolith production from the impact cratering record indicates a fine-grained regolith 3–17 m thick, overlying a coarse breccia that grades into jointed bedrock (Fig. 1). Mapping of surface terrains in high-resolution images of the landing site and surrounding areas shows these terrains are dominantly formed by impact and aeolian processes.

To complement the data of Table 1, a series of tests was carried out to investigate the mechanical properties of three different Mars regolith simulants with respect to the interactions between the InSight devices and the surface of Mars. Besides standard soil mechanics tests investigating the compressibility and the shear properties of the simulants, the measurements of seismic velocities were also conducted in link with the requirements related to the SEIS seismometer.

Fig. 1 HiRISE image (25 cm/pixel) showing ~ 10 m thick, fine grained regolith on top of coarse breccia overlying strong, jointed bedrock (Golombek et al. 2013, 2016)



3 Materials and Methods

3.1 Materials

The choice of the simulants was driven by the desire to reasonably bound the range of parameters expected on Mars as described in Golombek et al. (2008), Herkenhoff et al. (2008) and Golombek et al. (2016) and in Sect. 2, more particularly in terms of density requirements, grain size distribution and friction angles (see Table 1). Three simulants were tested: the Mojave simulant, provided by JPL and the Eifelsand and MSS-D (Mars Soil Simulant-D) simulants, both provided by DLR.

The simulants can be observed in the photos of Fig. 2, in which the fraction smaller than 2 mm has been separated from coarser grains. The Mojave simulant is a mixture of material used for testing mobility in the Jet Propulsion Laboratory's Mars Yard. It is composed of Mojave Mars Simulant (MMS), a widely used Mars simulant, which is crushed Miocene basalt from the Mojave Desert in Southeast California (Peters et al. 2008), alluvial sedimentary and igneous grains from the local area, and basaltic pumice that can be observed in the coarse fraction in Fig. 2. The Eifelsand simulant is a mix comprising pumice grains from the Eifel Mountains in Western Germany (a site with Tertiary and Quaternary volcanic activity) and crushed basalt grains. The grains larger than 2 mm observed in Fig. 2 are basalt pumice from the natural Eifelsand, with a small density and angular shapes. MSS-D is a fine grained mix made of 50% artificially ground olivine powder and 50% quartz. It is composed of silt and clay sized particles, that are finer than sand, and overlap the size of dust on Mars. As shown Fig. 2, both Mojave and Eifelsand simulants contain some particles too large to be tested in standard soil mechanics devices. Both simulants were sieved and only the fraction smaller than 2 mm was used to prepare the cylindrical triaxial specimens, the oedometer and the shear box specimens tested in this work.

The grain size distribution curves of the three simulants are presented in Fig. 3. They were obtained by sieving for Mojave and Eifelsand simulants and by both sieving and sedimentometry for MSS-D. The curves indicate that the fraction smaller than 2 mm in both Mojave and Eifelsand simulants are somewhat comparable (from fine sand to sand), with however a greater percentage of smaller particles in the Mojave simulant. The grain size distribution curve of Mojave is continuous, whereas the mix between smaller crushed basalt grains and larger volcanic pumice grains is perhaps detectable in Eifelsand at the inflection

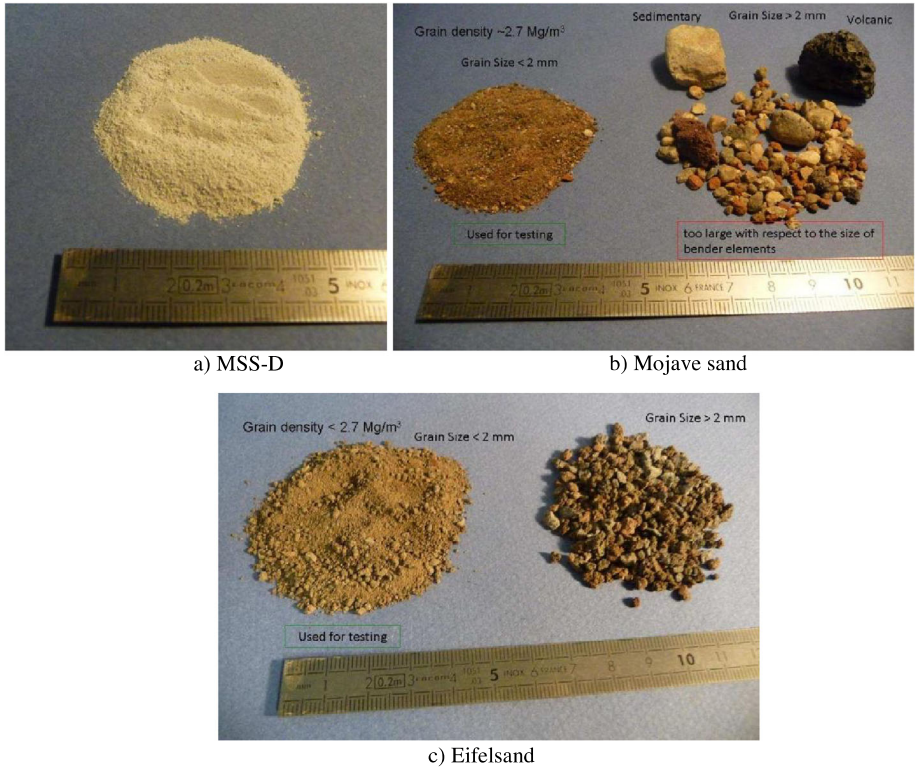


Fig. 2 Regolith simulants tested

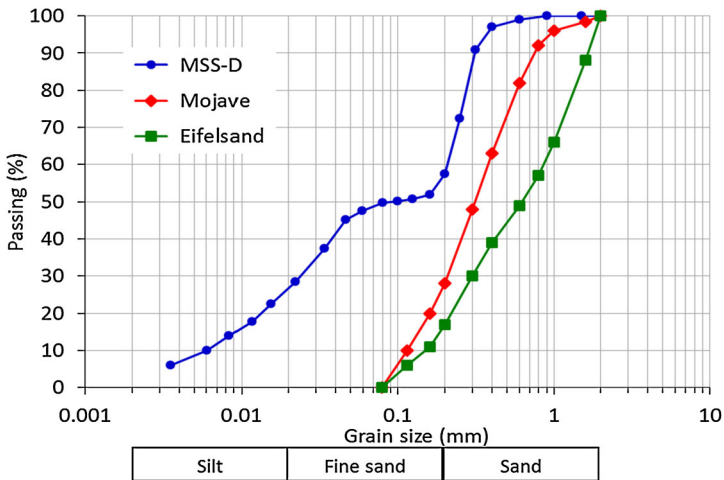


Fig. 3 Grain size distribution of the Martian simulants

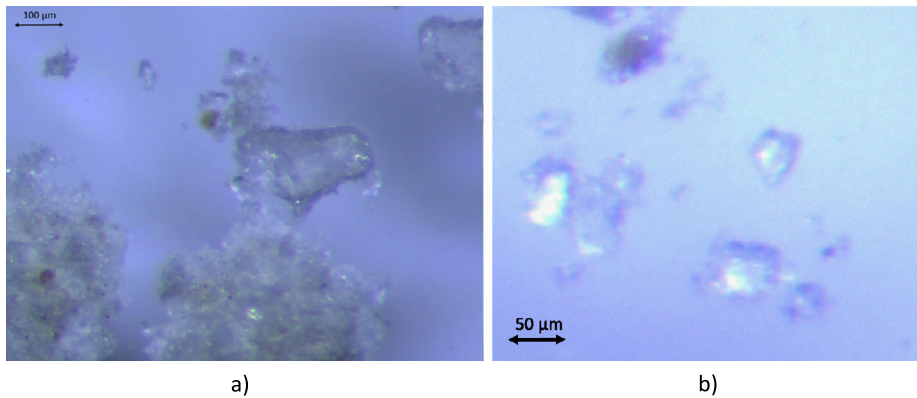
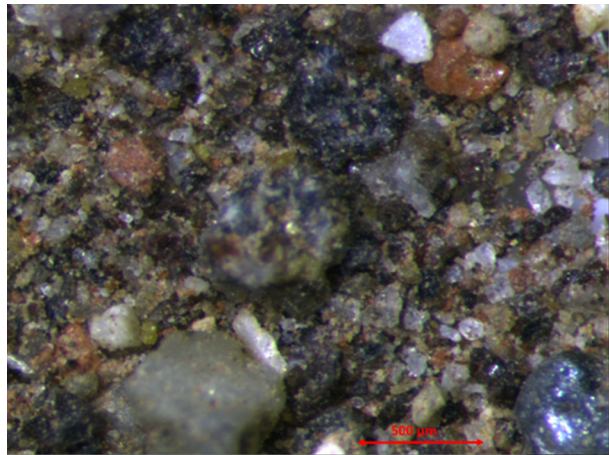


Fig. 4 Optical microscope observation, MSS-D: (a) quartz grain (around $150 \times 100 \mu\text{m}$) with aggregated crushed olivine particles; (b) crushed olivine particles

Fig. 5 Optical microscope observation, Mojave simulant (fraction $< 2 \text{ mm}$)



point at $500 \mu\text{m}$. The grain size distribution of MSS-D is clearly bi-modal, with clear evidence of both the 50% sand fraction (larger than $100 \mu\text{m}$) and the 50% fraction of crushed olivine (smaller than $100 \mu\text{m}$). The grain size is significantly smaller in MSS-D, in the silt range. It includes dust-size particles that fall from suspension in the Mars atmosphere and coat the surface at the landing site, but are not expected to form much of the soil beneath.

Further information on the simulants is now provided from optical microscope observations of their fine fraction ($< 2 \text{ mm}$). The photos of Fig. 4 were taken on MSS-D. Figure 4a shows a rounded quartz grain ($280 \mu\text{m}$ long and between 100 and $150 \mu\text{m}$ large) close to an aggregation of much finer and angular particles of crushed olivine. Figure 4b shows in more detail the angular shape of the crushed olivine particles. The largest ones have diameters around $50 \mu\text{m}$ and the others are around $20 \mu\text{m}$ or even less (particles as small as $2 \mu\text{m}$ have been detected at higher magnitude), in good agreement with the grain size distribution curve.

The $< 2 \text{ mm}$ fraction of Mojave is shown in Fig. 5. One clearly distinguishes the crushed sub-angular basalt grains, with diameters of hundreds of micrometers, from the grains of natural origin that comprise some clear quartz grains, and some salmon pink grains, likely

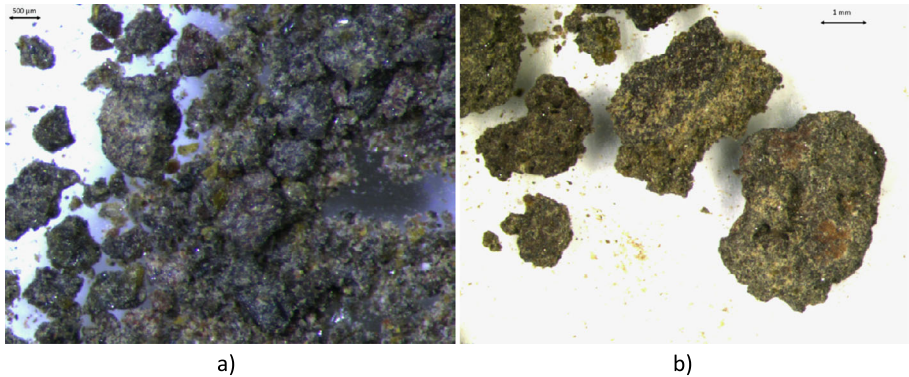


Fig. 6 Optical microscope observation, Eifelsand simulant (fraction < 2 mm): (a) smallest crushed basalt grains; (b) largest pumice grains

to be potassium feldspar. Small green grains are likely olivine from the basalt. Olivine inclusions are also observed in the basalt grain in the center of the photo.

The smallest grains (< 600 μm) of the Eifelsand simulant are observed in Fig. 6a and the largest ones (larger than 1 mm) in Fig. 6b. The grains in Fig. 6a are crushed dark basalt grains quite similar to that observed in the Mojave simulant, with some green olivine minerals that are either embedded in the basalt grains or separated by grinding. Conversely, the larger grains of Fig. 6b are pumice grains from the volcanic natural Eifelsand, with irregular and angular forms.

The solid densities of the individual particles ρ_s were determined by using a pycnometer and the following values were obtained:

- MSS-D: $\rho_s = 2.70 \text{ Mg/m}^3$
- Mojave sand: $\rho_s = 2.79 \text{ Mg/m}^3$
- Eifelsand: $\rho_s = 2.51 \text{ Mg/m}^3$

As expected from macroscopic observation, the density of the Eifelsand simulant (2.51 Mg/m^3) is smaller than that of both MSS-D and Mojave simulants, that are typical of most terrestrial minerals (including silica and calcite). The average density of the mix of crushed basalt grains and volcanic pumice grains constituting the Eifelsand simulant is significantly smaller than the density of basalt grains (2.8 Mg/m^3), because of the low density of the pumice grains.

3.2 Experimental Devices

Some mechanical tests were carried out in standard soil mechanics devices, including a direct shear box (6 cm side square box, 2 cm height) and a oedometer (diameter 70 mm, height 26 mm). Seismic velocity measurements were conducted in cylindrical specimens (50 mm diameter and 100 mm height) submitted to various isotropic confining stresses within a tri-axial cell.

When testing any granular material, special attention was paid to the density of the granular assembly, a paramount parameter that governs the overall response of granular materials, both in volumetric and shear aspects. Specimens were made up by carefully pouring the grains in the devices used (oedometer ring, shear box, cylinder for the triaxial sample) in an attempt to make homogeneous and regular specimens. Only one layer was used to fill the

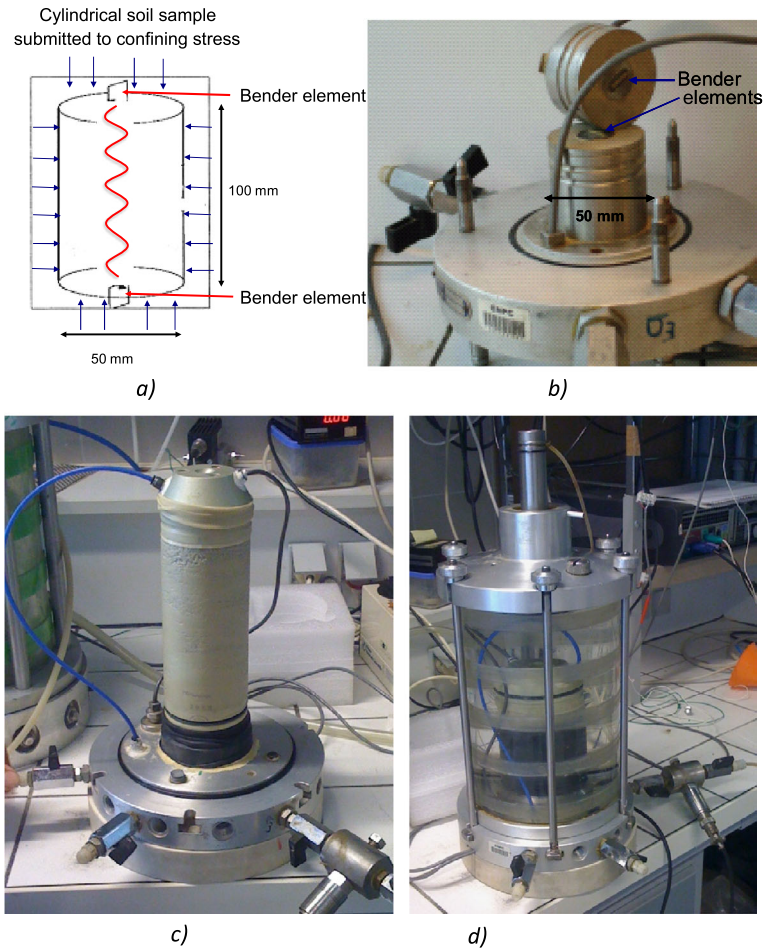


Fig. 7 Measurement of compression and shear seismic waves by means of bender elements

oedometer ring whereas the shear box specimen was made by pouring 3 successive layers of 20 mm height. The top surface of each layer was carefully regulated to obtain a plane of a constant height before pouring the following layer. The final density obtained was calculated from the specimen volume and mass.

The seismic velocities were measured by using bender elements, made up of piezoelectric ceramic plates working in frequency between 1 and 100 kHz. Bender elements are able to generate and receive both shear and compression waves once inserted in top and bottom of granular specimens. Figure 7 shows the principle of the measurement (a), with a photo of the bender elements inserted in the top and bottom caps (b), with the specimen mounted with both caps (c) and placed in the triaxial cell to apply isotropic stress once the cell is filled with water and water put under pressure (d). The size of the specimen (50 mm diameter and 100 mm height) was chosen larger than that of standard triaxial specimens (38 mm diameter and 76 mm height) so as to improve the precision of the measurements with a larger wave propagation distance along the axis of the specimen. Specimens were kept dry during the tests, conducted with a maximum applied confining pressure of 500 kPa.

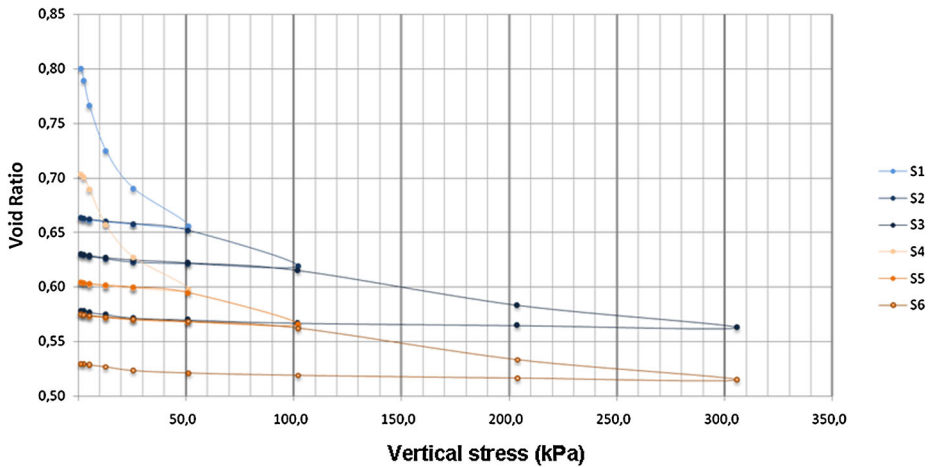


Fig. 8 Compression curves of the MSS-D simulant regolith

4 Experimental Results

4.1 Compression Curves

The one-dimensional oedometer compression curves of the three regoliths tested are presented in terms of changes in void ratio e with respect to changes in vertical stress σ_v . The void ratio is defined as the ratio between the volume of voids V_v with respect of the volume of the solid phase V_s ($e = V_v / V_s$).

Figure 8 presents the oedometer compression curves of MSS-D. Two tests were run on samples poured in the oedometer ring at two initial void ratios $e = 0.7$ and 0.8 that correspond to porosities n ($n = V_v / V$ where V is the total volume, with $V = V_v + V_s$) of 44.4 and 42.1% and to densities of 1.59 and 1.5 Mg/m³, respectively. Some stress cycles were carried out to make the distinction between elastic (reversible) strains and plastic (irreversible) strains, starting from vertical stresses of 50 and 100 kPa.

The compression curve shows how the compressibility, represented by the slope of the curve, is decreasing with increased stress and plastic densification (a denser assembly of grains is more difficult to compress). Significant plastic compression strain is mobilized between 0 and 50 kPa. The responses to the load cycles (50–0–50 kPa and 100–0–100 kPa) are fairly reversible with elastic strains much smaller than the previously mobilised plastic strains. The slopes of the elastic response above 50 kPa are fairly linear and equal. A slight curvature of the elastic response is observed between 0 and 25 kPa.

The same data are given for Mojave simulant in Fig. 9 for two tests conducted with initial void ratios of 0.683 and 0.764 corresponding to porosities of 40.5 and 43.3% and densities of 1.60 and 1.53 Mg/m³ respectively. Responses are comparable to that obtained on MSS-D with however significant less compression in the range 0–50 kPa, indicating lower compressibility.

Figure 10 provides the compression curves of Eifelsand simulant at two initial void ratios of 1.19 and 1.07 respectively. Void ratios are here significantly larger.

Figure 11 presents in a linear plot the changes in density with respect to the applied vertical stress. One observes that the initial density of Mojave simulant and MSS-D are close (given that they have same solid density, they have same porosity). The smaller initial

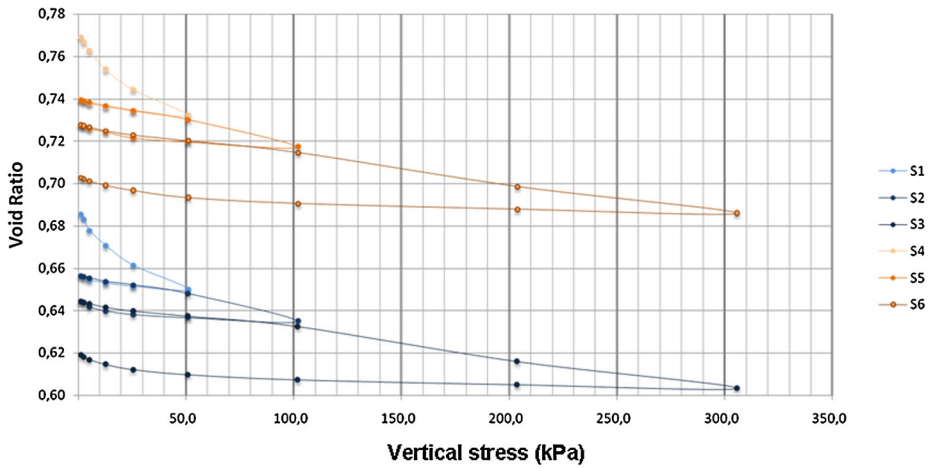


Fig. 9 Compression curves of the Mojave regolith stimulant

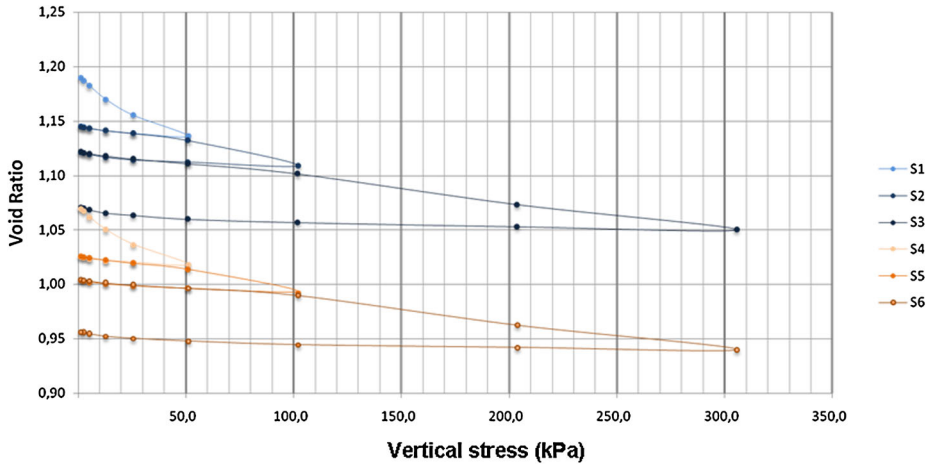


Fig. 10 Compression curves of the Eifelsand regolith stimulant

density of the Eifelsand sample is related to the smaller density of the solid grains. The curves also show that both Eifel and Mojave sands have comparable compressibility.

In an infinite horizontal half space under Mars gravity (taken equal to 3.71 m/s^2), a density of 1.5 Mg/m^3 (close to the initial density of Mojave and MSS-D) corresponds to a unit weight of 5.57 kN/m^3 and the weight of a 1 m thick layer exerts a vertical stress of 5.9 kPa. The 0–50 kPa stress range hence corresponds to vertical stresses between surface and 8.5 m deep to be compared to the 5 m maximum depth of the HP³ mole penetration. Compression test results hence provide an indication on the regolith density profile with respect to depth under the hypothesis of having the corresponding density at surface (1.5 Mg/m^3). Note that the technique of gently pouring the sand into the oedometer ring is known to provide rather loose specimens. The 1.5 Mg/m^3 value is however close to the maximum regolith surface density provided in Table 1 by Golombek et al. (2008). Also, the 1.5 Mg/m^3 value was

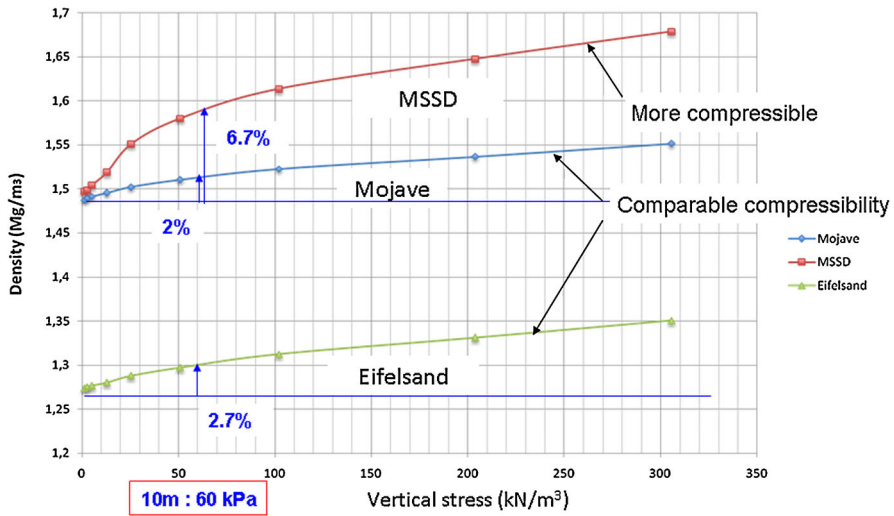


Fig. 11 Compression curves of the three regolith simulants tested

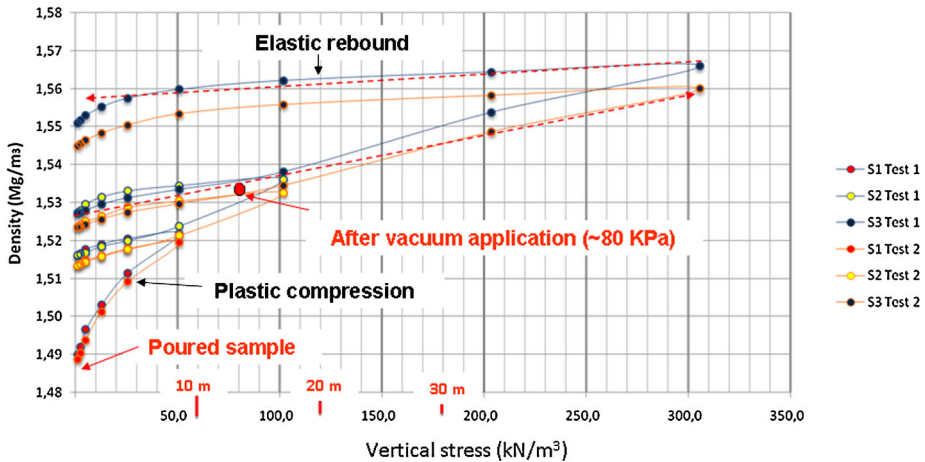


Fig. 12 Elasto-plastic response of Mojave sand

obtained under the Earth’s gravity and a smaller value could be expected under the Mars gravity. A smaller density at surface should then correspond to a larger compressibility and a larger increase in density with depth, as exhibited here by the MSS-D specimen.

The elasto-plastic compression response of Mojave simulant was further investigated in the oedometer by carrying out two similar tests in which stress cycle were successively applied as follows: 0–50–0 kPa followed by 0–100–0 kPa and then 0–300–0 kPa. The data obtained (Fig. 12) show good repeatability between test 1 and test 2. The difference between plastic larger strains, upon the first stress application at levels never supported before by the grain assembly (resulting in significant modification of the assembly), compared to smaller elastic strains, when stress cycling at values smaller than the maximum stress previously applied (no significant reorganisation of grain assembly), is clear, with maximum plastic

strain obtained during the first compression between 0 and 50 kPa. The elastic rebound and loading curves are reasonably comparable with the slopes of the various cycles reasonably parallel, as typically observed in sands and other soils.

Starting from the initial density of 1.49 Mg/m^3 of the poured specimen, the point at 80 kPa with a density of 1.532 Mg/m^3 is of particular interest since it corresponds to the application of vacuum that will be performed when making the triaxial sample, as described further on.

4.2 Shear Test Results

The direct shear box data obtained on Mojave and Eifelsand simulants at a density of 1.57 Mg/m^3 are presented together in Fig. 13 in terms of changes of tangential stress τ (kPa) and volume (from the changes in height of the specimen Δh , mm) with respect to the relative displacement between the two half-boxes (mm). On each sample, tests have been duplicated with satisfactory reproducibility between the repeated tests. The curves of the tests carried out under vertical loads of 29, 58, 116 and 231 kPa are presented.

The shape of the shear stress curve is typical of moderately loose sands with no marked peak at maximum shear stress but an increase in shear stress with displacement leading to progressive stabilisation. The maximum stresses reached in both case are comparable, although a little higher for Eifelsand. In Mojave simulant, the volume change indicates a contraction increasing with stress, typical of loose sands. The transition between contracting and dilating behaviour occurs in all cases after 2 mm. The contracting behaviour is less marked in Eifelsand with a transition from contraction to dilation occurring at smaller displacement (0.6 mm) under 29 kPa. Note however that the maximum contraction observed under 231 kPa is higher than previously and corresponds to 0.6 mm. The shape of the volume change curves is more regular compared to Mojave simulant where volume changes were apparently affected by some friction effects in the LVDT monitoring changes in height during shear.

Figure 14 shows same data for MSS-D in which no stabilization is observed in shear stress, but a constant increase in shear, particularly at stresses of 116 and 231 kPa. This occurs with constant contracting trend, not very sensitive to stress, with a maximum of 0.6 mm under the highest stress. This contracting response is linked to the larger compressibility observed in Fig. 11. The progressive increase in shear stress is linked to the constant volume decrease observed on the sample that gets stronger by increased density.

The corresponding friction angles at the density of 1.57 Mg/m^3 are given in Fig. 15, with the highest value of 42° obtained for Eifelsand compared to 38° for Mojave and 35.5° for MSS-D. The significantly higher friction angle of Eifelsand at same density is probably due to higher grain angularity, in particular because of the shape of the pumice largest grains. Note however that in spite of having 50% of angular crushed olivine, MSS-D exhibits the smallest angle of 35.5° , probably thanks to the rounded shape of the 50% sand grains.

Compared to the data of Table 1, the values of friction angle are larger, in relation with the larger dry density obtained in this work by pouring (1.57 Mg/m^3 compared to a maximum value of 1.3 Mg/m^3 given in Table 1). As will be commented later, smaller friction angles are expected at lower density.

4.3 Seismic Velocities

Figure 16 shows the changes in velocities with respect to the isotropic confinement stress both in terms of compression (a) and shear (b) waves for Mojave sand. These data come

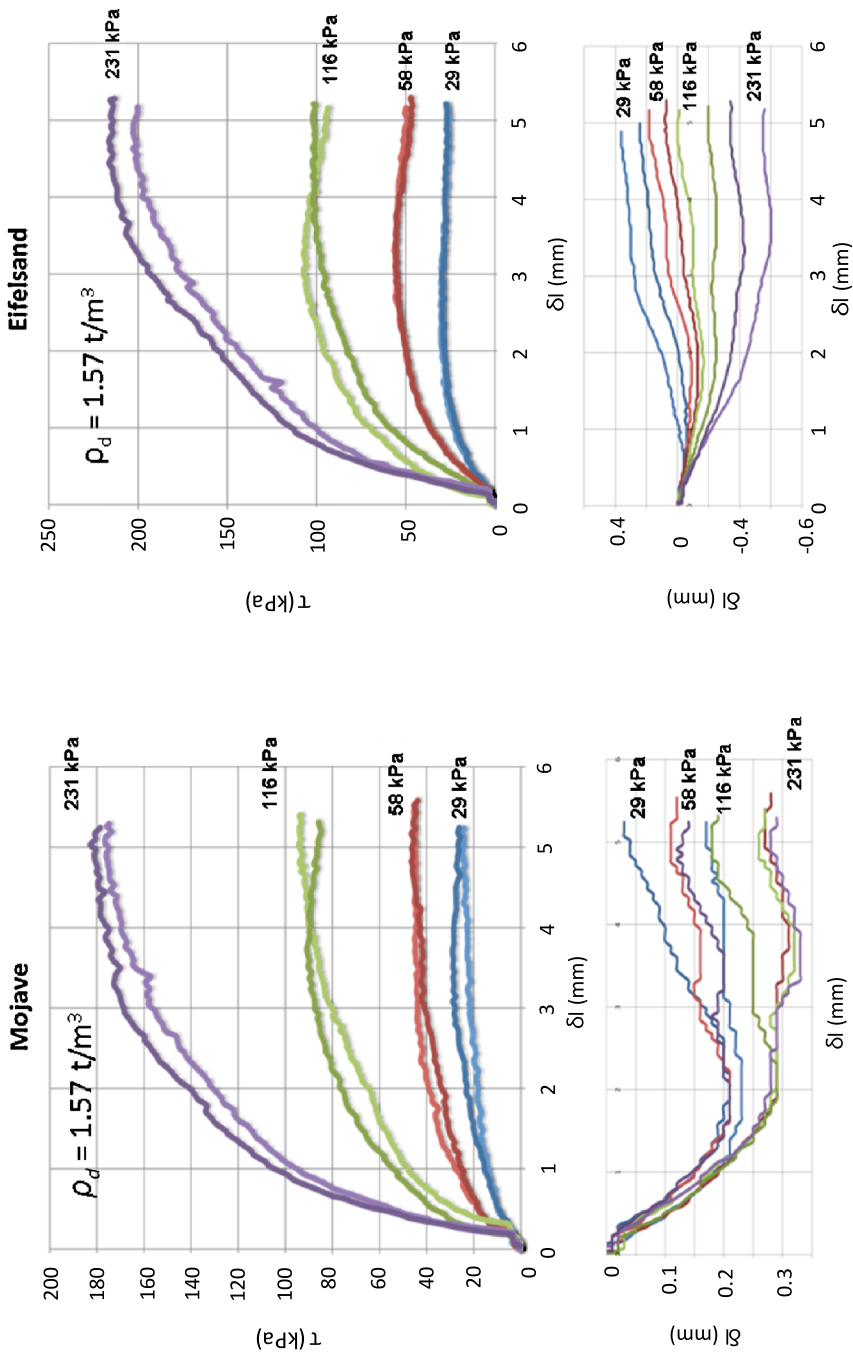


Fig. 13 Shear tests results, Mojave and Eifelsand

Fig. 14 Shear tests results, MSS-D

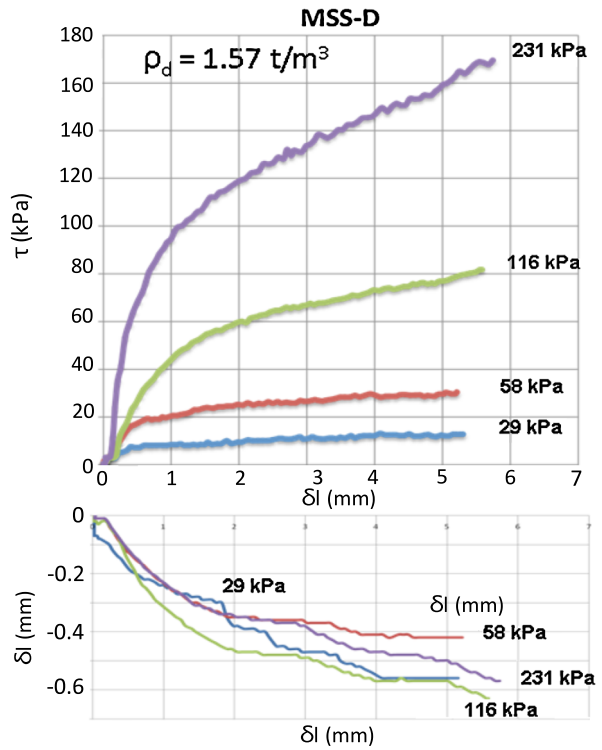
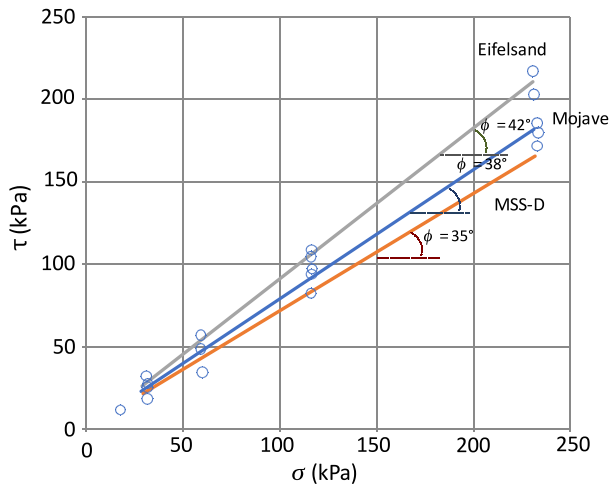


Fig. 15 Friction angles



from various measurements carried out in two tests along various stress paths comparable to that followed to investigate the elasto-plastic response of Mojave simulant in Fig. 12. A first series of measurements was carried out under stresses of 25, 50 and 100 kPa, mobilising the elasto-plastic strains observed in Fig. 12 along a monotonic loading path. The sample was afterwards elastically unloaded at 25 kPa and loaded again under 50, 100, with subsequent

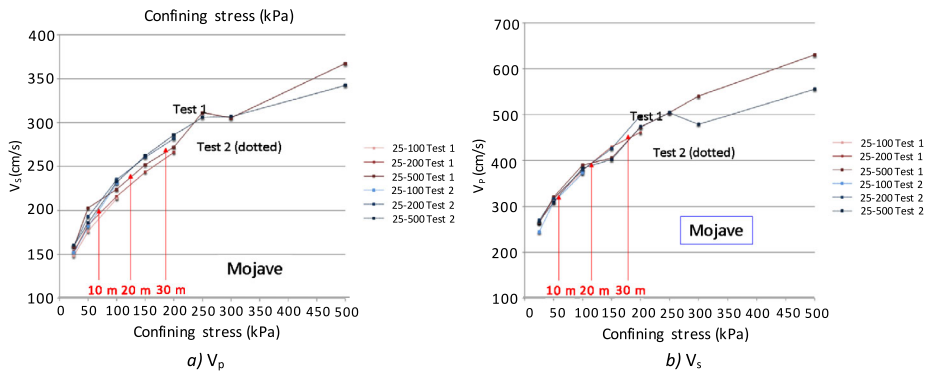


Fig. 16 Changes in seismic velocity with respect to isotropic confining stress, Mojave sand: (a) V_p ; (b) V_s

plastic compression up to 200 kPa. Finally, an elastic unloading/reloading stage at 25, 50, 100 and 200 kPa was followed by an elasto-plastic compression at 300 and 500 kPa. The corresponding depths of interest (10, 20 and 30 m) are also indicated in the graph. Note that, compared to the oedometer tests in which the vertical stress was imposed (with a lateral stress response resulting from the no radial strain condition, a condition typical of oedometer), the stresses applied here are isotropic.

Interestingly, there is no effect of stress cycles and hence of the nature either plastic (first stress application) or elastic response along the compression strain (see Fig. 12) on the values of the seismic velocities. The increase in velocity is more sensitive to the increase in inter-granular forces resulting from the increase of confining stress than to the increase in density. The data of a given test along the three successive stress paths are in good agreement. There is also good agreement between the two tests carried out on two different specimens (except at high stress for V_p).

One can see that there is a non-linear increase in compression wave velocity with the applied stress from approximately 250 m/s at low stress (25 kPa corresponding to a depth of 5 m) to around 600 m/s under 500 kPa. As expected, shear waves are smaller than compression waves with comparable trends, providing a reliable estimation of the changes in velocity with depth.

Similar trends are observed for MSS-D and Eifelsand. The comparison of the data from the three simulants shown in Fig. 17 confirm their comparable responses in velocity with respect to changes in applied stress, with larger values and stronger increase observed on the MSS-D specimen, of a different nature (crushed powder). The two fractions smaller than 2 mm of the Mojave and Eifelsand simulants, both in the grain size range of sand, provide comparable results in terms of changes in seismic velocity with confining stress.

5 Discussion

The data obtained are now discussed with respect to the data provided by Golombek et al. (2008, 2016) and presented in Table 1. In terms of grain size distribution (Fig. 3), the particles of the MSS-D powder are larger than the “Drift” and smaller than “Sand bedforms”, whereas Mojave and Eifelsand simulant (most particles between 0.1 and 1 mm) are included in the range of the “Blocky, Indurated Soil”.

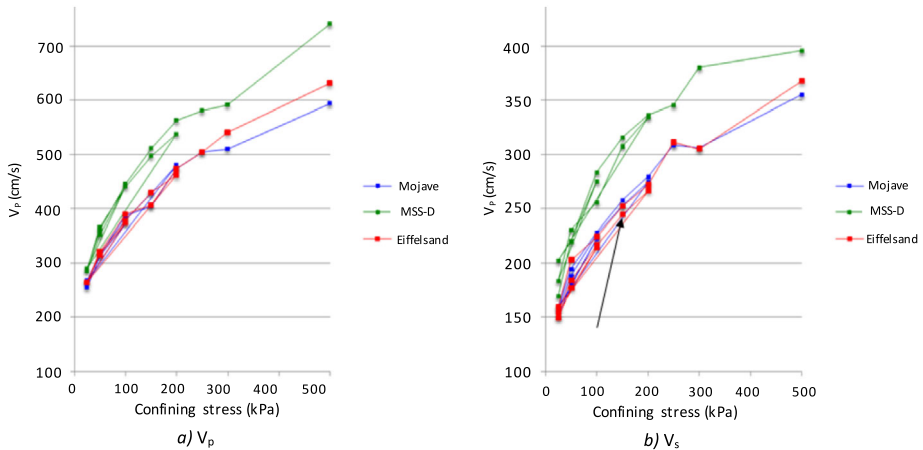
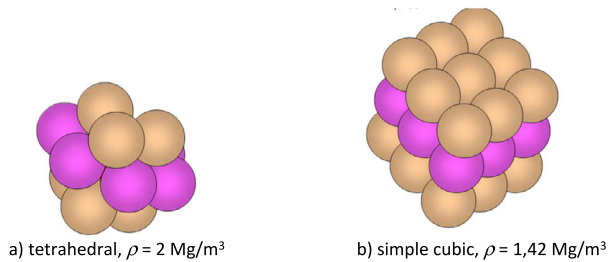


Fig. 17 Comparison of seismic velocities on the three specimens

Fig. 18 Effect of the geometrical assembly of spheres of same diameter on the density



Beside the grain size distribution, density strongly affects the mechanical properties of sands, with larger friction angles in denser sands, that exhibit expansion under shear due to the disentangling of the particle assembly. Looser sands have lower friction angles with contraction during shear, due to tangling.

5.1 Possible Density Values

Some further considerations concerning possible density values for regolith at the surface of Mars can be drawn from geometrical considerations, that have been summarised in Santamarina et al. (2001). A simple illustration providing first order estimates can be obtained by considering an assembly of spherical particles of the same diameter in the densest possible arrangement (called tetrahedral) as shown in Fig. 18a, with a minimum void ratio $e_{min} = 0.351$ corresponding to a maximum density of 2 Mg/m^3 (a rather high density for granular soils). Conversely, the loosest possible assembly (simple cubic) is depicted in Fig. 18b, with a maximum void ratio $e_{max} = 0.908$ and a minimum density of 1.42 Mg/m^3 .

The situation of natural sand is of course more complex with significant effects of both the grain size distribution (non-uniform grain size distribution can provide denser assemblies, with smaller grains inserted in the voids between larger ones) and the real grain shape (irregular angular grains may provide looser assemblies than regular rounded ones). This is illustrated by the data of Table 2 (Bolton 1986) that provides the minimum and maximum void ratios (e_{min} and e_{max} , respectively, obtained by following normalised procedures) and

Table 2 Typical void ratios and densities of terrestrial sand (after Bolton 1986)

Sand name	D_{60}	D_{10}	e_{min}	ρ_{max} (Mg/m ³)	e_{max}	ρ_{min} (Mg/m ³)
Brasted river	0.29	0.12	0.47	1.84	0.79	1.51
Mersey river	0.2	0.1	0.49	1.81	0.82	1.48
Monterey N°20	0.3	0.15	0.57	1.72	0.78	1.52
Monterey N°0	0.5	0.3	0.57	1.72	0.86	1.45
Ham river	0.25	0.16	0.59	1.70	0.92	1.41
Leighton Buzzard 14/25	0.85	0.65	0.49	1.81	0.79	1.51
<i>Welland river</i>	0.14	0.1	0.62	1.67	0.94	1.39
<i>Chattahoochee river</i>	0.47	0.21	0.61	1.68	1.10	1.29
Mol	0.21	0.14	0.56	1.73	0.89	1.43
Berlin	0.25	0.11	0.46	1.85	0.75	1.54
Guinea marine	0.41	0.16	0.52	1.78	0.9	1.42
Portland river	0.36	0.23	0.63	1.66	1.1	1.29
<i>Glacial outwash sand</i>	0.9	0.15	0.41	1.91	0.84	1.47
Karlshue medium sand	0.38	0.2	0.54	1.75	0.82	1.48
Sacramento river	0.22	0.15	0.61	1.68	1.03	1.33
Ottawa sand	0.76	0.65	0.49	1.81	0.8	1.50

densities that characterize a series of terrestrial sands defined by their diameters D_{60} (60% of the grains have diameter smaller than D_{60}) and D_{10} (10% of the grains have diameter smaller than D_{10}). One can see that the loosest sands (Welland river and Chattahoochee river) have smallest densities equal to 1.39 and 1.29 Mg/m³, respectively. Note that river sands are known to be rather rounded due to transportation in water, in contrast to sand on Mars that is rounded in saltation (McGlynn et al. 2011). For the same grain size distribution, less rounded grains would result in slightly higher density.

The largest density is obtained with the glacial outwash sand (1.91 Mg/m³). Note that both the minimum and maximum density values are not too far from that obtained from simple geometrical considerations on ideal granular assemblies of spheres in Fig. 18. In terms of grain size distribution, one can observe that sands with average diameter of 0.2 mm (Brasted river, Monterey N°20, Ham river and Berlin) have minimum densities comprised between 1.41 (Ham river) and around 1.52 Mg/m³ (Brasted river, Monterey N°20, and Berlin). These density values are of the same order of magnitude as that adopted in the tests carried out in this work. Another important factor influencing the morphology of granular assemblies is gravity, and it is likely that the smaller gravity on Mars (3.711 m/s²) should result in looser assemblies of grains of same shape and size distribution compared to the gravity on Earth (9.807 m/s²). Both effects of smaller roundness and gravity are compatible with the fact that the 1.3 Mg/m³ value provided in Table 1 is smaller the 1.41–1.52 Mg/m³ density values estimated from terrestrial sands.

5.2 Possible Values of the Friction Angle

The changes in friction angle with respect to density obtained from triaxial tests on the Sacramento river sand (Lee and Seed 1967) are presented in Table 3, confirming the important effect of density on the friction angle, with an increase in friction angle with density from 34° in loose state to 41° in dense state.

Table 3 Change in friction angle with respect to density, Sacramento river sand (after Lee and Seed 1967, in Holtz and Kovacs 1981)

State	Void ratio e	Density (Mg/m^3)	Friction angle
Loose	0.87	1.44	34°
Moderately loose	0.78	1.52	37°
Moderately dense	0.71	1.58	39°
Dense	0.61	1.68	41°

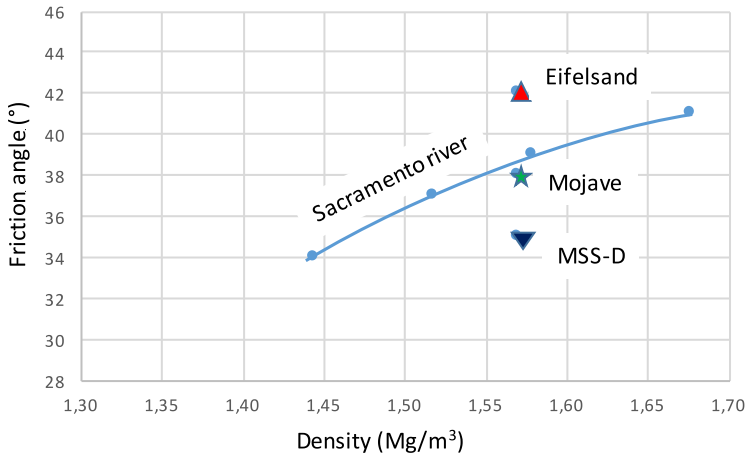


Fig. 19 Changes in friction angle with respect to density: Sacramento river sand (Lee and Seed 1967) and the tested regoliths

These data are compared to that of the regolith simulants studied in this work in Fig. 19. This comparison between friction angle from triaxial tests (Sacramento river) and direct shear box (Regolith simulants) is somewhat approximate, but it is deemed to provide reasonably good trend in terms of orders of magnitude. The friction angles obtained at a density of $1.57 \text{ Mg}/\text{m}^3$ (Fig. 15) are equal to 35° for MSS-D, 38° for Mojave and 42° for Eifelsand. There is good agreement between the data of Mojave simulant with that of the Sacramento river sand at $1.57 \text{ Mg}/\text{m}^3$.

Based on the shape of the curve, it seems reasonable to consider that angles around $28\text{--}30^\circ$ correspond to a density of $1.3 \text{ Mg}/\text{m}^3$, confirming the value given in Table 1.

5.3 Dynamic Penetration

The response of the regolith to the dynamic penetration of the mole of the HP³ device is an important issue, investigated by running full size penetration tests in the JPL and DLR facilities. Dynamic penetration in sands is complex, involving dynamic sand/mole interactions, large axisymmetric strains and the contracting-dilating shear behavior of the sand (see Figs. 13 and 14). Dense sands will expand under shear around the cone, resulting in an increase in normal stresses along the mole, whereas the contraction of loose sands will result in a release in normal stresses, making penetration easier.

In spite of the availability of advanced constitutive elastoplastic models of sands that correctly model the shear volume changes with respect to sand density, there is still a need to progress in the numerical modelling of dynamic penetration, due to the difficulty of using

large strains calculations and to correctly account for dynamic effects. Modelling correctly dynamic penetration would allow to back analyze the penetration of the mole in the landing site, providing useful parameters to characterize the first 5 m layer of the regolith penetrated by the mole.

The procedure used to make the sand column in which the full-scale penetration tests are run and the resulting density profile are quite important. It is likely that tests run under Earth's gravity will result in higher density profile compared to tests under Mars' gravity. Smaller densities (around 1.3 Mg/m^3) would result in a contracting response, tending to make penetration easier. The response to penetration that will be monitored during the penetration of the mole will hence provide a valuable response that could be compared to penetration tests that would be run at various densities on Earth, in an attempt to get the same response. Ideally, some information about the change in density with depth could then be obtained.

5.4 Seismic Velocities

An important conclusion drawn from the data of Fig. 17 is that the seismic velocities are not too sensitive with respect to the sand density within the range involved during the test, that can be estimated for Mojave simulant from the compression test of Fig. 11. Seismic velocities should mainly depend on the confining stress along the 10 meters depth estimated at the landing site (density increases for Mojave simulant from 1.488 to 1.523 Mg/m^3). It is also interesting to see that, in spite of their differences, Eifelsand and Mojave simulants exhibit comparable changes in seismic velocity with the confining stress. Also, there is a convergence with the velocities in MSS-D at low stress, in spite of significant difference in the grain size distribution.

The changes in compression wave with respect to shear wave are presented in Fig. 20. The three simulants exhibit comparable curves, and an average and reliable estimation of the Poisson ratio can be made by using Eq. (1), providing a value $\nu = 0.22$.

$$\frac{V_p}{V_s} = \sqrt{\frac{2(1-\nu)}{1-2\nu}} \quad (1)$$

The changes in seismic velocities with respect to the confining stress (σ_c) is defined by an empirical law (see Santamarina et al. 2001), as follows:

$$V = \alpha \left(\frac{\sigma'_0}{1 \text{ kPa}} \right)^\beta \quad (2)$$

in which α and β are experimentally determined. α is the velocity of the medium subjected to 1 kPa confinement. As recalled by Santamarina et al. (2001), the stiffer the particles and the denser the packing, the higher the value of α and the lower the β exponent. Theoretical values of β are $1/6$ for Hertzian contacts between elastic spherical spheres, $1/4$ for cone to plane contacts (typical of rough or angular particles) and $1/4$ for spherical particles with yield. Values between 0.12 and 0.28 are reported for sands.

As seen in Fig. 21, the best fitting with the data of this work was obtained with an exponent β equal to 0.3. As seen in the figure, this fitting provides an estimate of the compressional wave velocity at the surface (zero stress) at around 150 m/s.

The calculation of the Young modulus based on the seismic velocities is given below:

$$E = \rho V_p^2 * \left(\frac{3 - \frac{4}{I^2}}{I^2 - 1} \right) \quad (3)$$

Fig. 20 Changes in V_p with respect to V_s for the three simulants tested

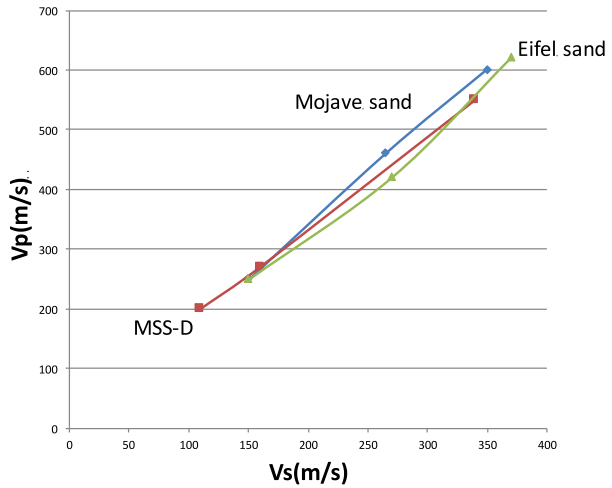
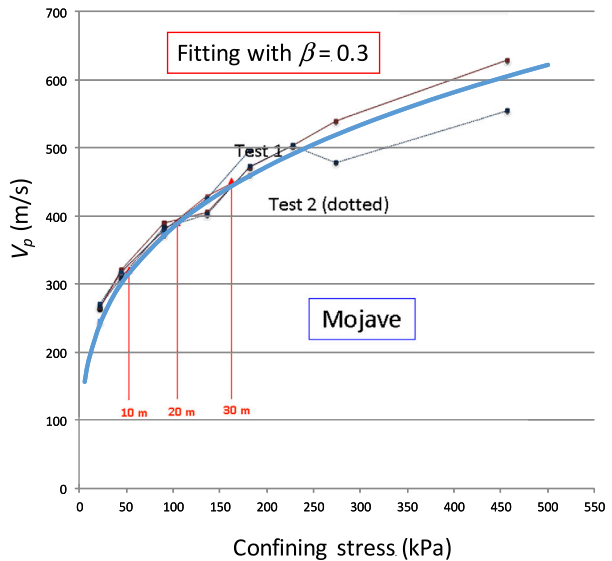


Fig. 21 Fitting the changes in seismic velocity with a power law, Mojave sand



Based on the value estimated from Fig. 21 at the surface, the value of the Young modulus is estimated at 51.2 MPa for a density of 1.533 Mg/m³ and 43.5 MPa for a density of 1.3 Mg/m³.

Extrapolation to the InSight landing site subsurface On Mars, the seismic and density of the near subsurface will in fact result from a mixture of rocks and soils, the later with seismic and density properties comparable to those of the simulants investigated in this study. In order to predict a possible ground model, one assumed 10% fraction of rocks, which corresponds to the upper bound of the requirement made on the landing site selection constraints (Golombek et al. 2016). Velocities of the ground were computed by assuming the ground as a mixture of rocks and soil and gravity of 3.711 m/s² for pressure increase. The ground seismic parameters were computed with the three different theories of Haskin-

Table 4 InSight Reference ground model for the upper layers dependence, for a bedrock deeper than 80 m

Depth	Density (Mg/m^3)	V_s	V_p
1–2 m	1.665	150 m/s	265 m/s
2–10 m	1.690	190 m/s	330 m/s
10–20 m	1.710	270 m/s	420 m/s
20–30 m	1.730	300 m/s	500 m/s
30–80 m	1.750	350 m/s	600 m/s

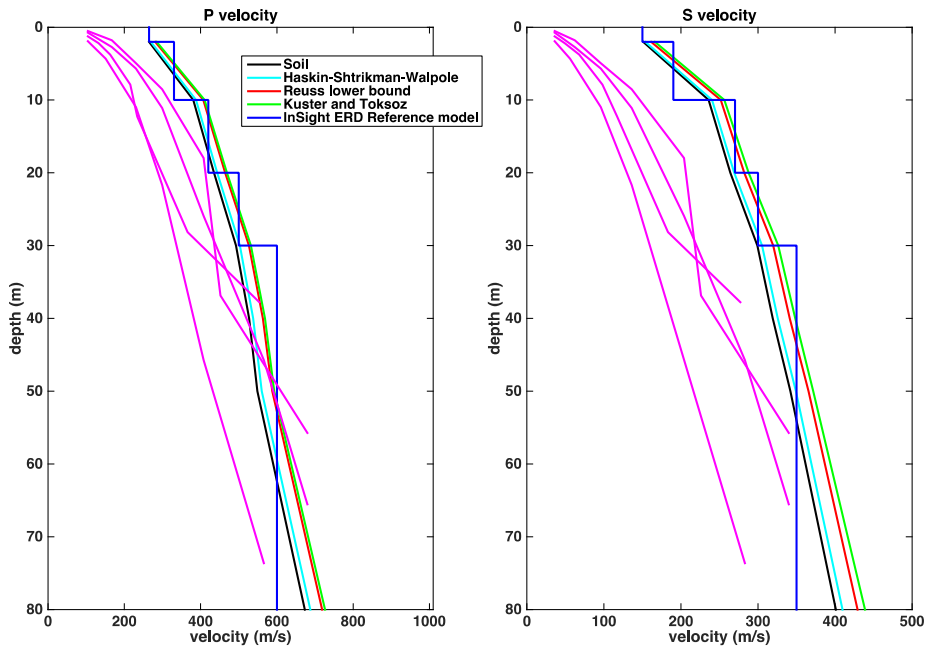


Fig. 22 Soil velocity as a function of depth, together with the estimation of the velocities for three different mixture theories. A 10% rocks composition is assumed. *Magenta curves* are the seismic velocities of Apollo sites A12, A14, A15, A16 when corrected with the gravity differences (i.e. shown at a Martian depth providing the same pressure as the lunar depth)

Shtrikman-Walpole, Reuss (lower bound) or Kuster and Tokzos, all described in Mavko et al. (2009). Rocks velocities and density are taken as 5000 m/s, 2800 m/s and 2.7 Mg/m^3 , respectively.

The model selected from these three different scenarios is provided in Table 4 and Fig. 22. This model has been used as reference for the Experiment Requirement Document (ERD). We get low velocities (265–420 m/s for V_p , 150–270 m/s for V_s) for the upper 15 meters. These velocities are significantly larger than those of the lunar regolith, also represented in the figure (Horvath et al. 1980) but are nevertheless low enough to favor significant wind induced deformations (Lognonné and Mosser 1993, Murdoch et al. 2016a, 2016b). These might be at long period the primary source of noise for the seismometer, as described in these papers.

6 Concluding Remarks

A series of mechanical tests were carried out on various Mars regolith simulants (MSS-D, Eifelsand and Mojave simulants) to help estimate the mechanical properties of the regolith at the landing site of the forthcoming InSight mission, in complement of previous estimations carried out from satellite observations and from local observations during previous missions. This investigation concerns the elastic interaction between the feet of the SEIS seismometer and the regolith, so as to further inform the noise model of the seismometer (Mimoun et al. 2016), including noise due to the wind (Murdoch et al. 2016a, 2016b). The estimation of the velocity of the seismic waves at the surface layer is another important issue.

The mechanical characteristics of the first 5 meters of regolith will govern the dynamic penetration of the mole of the HP³ device, that will be strongly affected by the density profile. Particular attention was hence devoted to the effects of density, given that standard techniques to get loose sand specimens in experiments under Earth's gravity probably over-estimate densities. The densities obtained in this work are 1.4–1.5 Mg/m³, larger than the 1.3 Mg/m³ density estimated at the surface of the landing site. At this density, direct shear box tests results and their comparison with data from terrestrial sands provided a value of friction angle around 30°, that will possibly increase if there is an increase in density in the first 5 m of the regolith layer. An estimation of this density gradient was provided by oedometer compression tests. In loose conditions, the penetration of the HP³ mole will mobilize contracting shear volume changes that should make the penetration easy, thanks to the resulting stress release around the penetrating mole. The monitoring of the penetration along the 5 m will certainly provide very useful information on the mechanical properties of the layer. Note however that the numerical modelling of dynamic penetration remains a difficult challenge and that the back analysis of the mole penetration will not be too easy.

The seismic velocities of the three regoliths simulants and their changes with respect to the confining stress applied were measured by using ceramic piezoelectric bender elements in triaxial specimens submitted to various stress paths. The data showed that the seismic velocities mainly depended on the (isotropic) stress applied, with no significant effect of the elasto-plastic strains induced by the applied stress path. Good compatibility was observed between the three regoliths, providing good confidence in the data obtained, with a compression wave velocity estimated at 150 m/s at the surface and a power law of the stress with an exponent of 0.3. With a 10% mixture with rocks, compression wave velocities were estimated at 265 m/s in the 0–2 m depth range and at 330 m/s in the 2–10 m range.

These mechanical parameters will be compared to the data obtained from the InSight mission, so as to better characterise the properties of the materials at the surface of the landing site.

Acknowledgements This work has been supported by CNES (the French space agency) and Ecole des Ponts ParisTech, within the frame of the SEIS/InSight project activities. The second author acknowledges the financial support of his Ph.D. provided by both the UnivEarthS Labex program at Sorbonne Paris Cité (ANR-10-LABX-0023 and ANR-11-IDEX-0005-02) and the SODERN company. Authors also acknowledge the support of NASA-JPL (T. Hudson) and DLR (M. Grott) for providing the Mars simulant samples and for their support to InSight activities. They also wish to thank J.M. Plessier, from Ecole des Ponts ParisTech, for his help in providing the optical microscope photos of the regoliths. This is InSight Contribution no. 21.

References

- K.A. Alshibli, M. Alsaleh, D.L. Godbold, E.J. Macari, Numerical and experimental study of strength properties of Martian regolith, *Earth & space 2004*, in *9th ASCE International Conference on Engineering, Construction, and Operations in Challenging Environments*, Houston, Texas (2004), pp. 1–8

- W.B. Banerdt et al., InSight: a discovery mission to explore the interior of Mars. in *44th Lunar and Planetary Science, Abstract #1915* (Lunar and Planetary Institute, Houston, 2013)
- M. Bolton, The strength and dilatancy of sands. *Geotechnique* **1**(36), 65–78 (1986)
- A. Becker, C. Vrettos, Tests on the thermal conductivity of regolith quasi-analogues at different porosities, in *Earth and Space 2016, 15th ASCE International Conference on Engineering, Science, Construction and Operations in Challenging Environments* (2016)
- W. Goetz et al., Microscopy analysis of soils at the Phoenix landing site, Mars: classification of soil particles and description of their optical and magnetic properties. *J. Geophys. Res.* **115**, E00E22 (2010). doi:[10.1029/2009JE003437](https://doi.org/10.1029/2009JE003437)
- M.P. Golombek, A.F.C. Haldemann, R.A. Simpson, R.L. Fergason, N.E. Putzig, R.E. Arvidson, J.F. Bell III., M.T. Mellon, Martian surface properties from joint analysis of orbital, Earth-based, and surface observations, in *The Martian Surface: Composition, Mineralogy and Physical Properties*, ed. by J.F. Bell III. (Cambridge University Press, Cambridge, 2008), pp. 468–497. Chap. 21
- M. Golombek, N. Warner, C. Schwartz, J. Green, Surface characteristics of prospective InSight landing sites in Elysium Planitia, in *44th Lunar and Planetary Science, Abstract #1696* (Lunar and Planetary Institute, Houston, 2013)
- M.P. Golombek et al., Selection of the InSight landing site. *Space Sci. Rev.* (2016, this Issue). doi:[10.1007/s11214-016-0321-9](https://doi.org/10.1007/s11214-016-0321-9)
- K.E. Herkenhoff, M.P. Golombek, E.A. Guinness, J.B. Johnson, A. Kusack, L. Richter, R.J. Sullivan, S. Gorevan, In situ observations of the physical properties of the Martian surface, in *The Martian Surface: Composition, Mineralogy and Physical Properties*, ed. by J.F. Bell III. (Cambridge University Press, Cambridge, 2008), pp. 451–467. Chap. 20
- R.D. Holtz, W.D. Kovacs, *An Introduction to Geotechnical Engineering* (Prentice Hall, New York, 1981)
- P. Horvath, G.V. Latham, Y. Nakamura, H. Dorman, Lunar near-surface shear wave velocities at the Apollo landing sites as inferred from spectral amplitude ratios. *J. Geophys. Res.* **85**, 6572–6578 (1980)
- S. Kedar, J. Andrade, B. Banerdt, P. Delage, M. Golombek, T. Hudson, A. Kiely, M. Knappmeyer, B. Knappmeyer-Endrun, C. Krause, T. Kawamura, P. Lognonne, T. Pike, Y. Ruan, T. Spohn, N. Teanby, J. Tromp, J. Wookey, Analysis of regolith properties using seismic signals generated by InSight's HP³ penetrator. *Space Sci. Rev.* (2017, submitted). InSight special issue
- K.L. Lee, H.B. Seed, Drained strength characteristics of drained sands. *J. Soil Mech. Found. Div.* **SM6**, 117–141 (1967)
- P. Lognonné et al., Science goals of the SEIS, the InSight seismometer package, in *46th Lunar and Planetary Science, Abstract #2272* (Lunar and Planetary Institute, Houston, 2015)
- P. Lognonné, T. Pike, in *Planetary Seismometry*, ed. by V.C.H. Tong, R.A. Garcia (Cambridge University Press, Cambridge, 2015)
- P. Lognonné, B. Mosser, Planetary seismology. *Surv. Geophys.* **14**, 239–302 (1993). doi:[10.1007/BF00690946](https://doi.org/10.1007/BF00690946)
- G. Mavko, T. Mukerji, J. Dvorkin, *The Rock Physics Handbook* (Cambridge University Press, Cambridge, 2009)
- I.O. McGlynn, C.M. Fedo, H.Y. McSween Jr., Origin of basaltic soils at Gusev crater, Mars, by aeolian modification of impact-generated sediment. *J. Geophys. Res.* **116**, E00F22 (2011). doi:[10.1029/2010JE003712](https://doi.org/10.1029/2010JE003712)
- D. Mimoun, M. Murdoch, P. Lognonné, T. Pike, K. Hurst (the SEIS team), The seismic noise model of the InSight mission to Mars. InSight Special Issue (2016)
- M. Murdoch, D. Mimoun, R.F. Garcia, W. Rappin, T. Kawamura, P. Lognonné, Evaluating the wind-induced mechanical noise on the InSight seismometers. InSight Special Issue (2016a)
- M. Murdoch, B. Kenda, T. Kawamura, A. Spiga, P. Lognonné, D. Mimoun, W.B. Banerdt, Estimations of the seismic pressure noise on Mars determined from Large Eddy. Simulations and demonstration of pressure decorrelation techniques for the InSight mission. *Space Sci. Rev.* (2016b, this Issue)
- G.H. Peters, W. Abbey, G.H. Bearman, G.S. Mungas, J.A. Smith, R.C. Anderson, S. Douglas, L.W. Beegle, Mojave Mars simulants—characterization of a new geologic Mars analog. *Icarus* **197**, 470–479 (2008). doi:[10.1016/j.icarus.2008.05.004](https://doi.org/10.1016/j.icarus.2008.05.004)
- S. Piqueux, P.R. Christensen, Temperature-dependent thermal inertia of homogeneous Martian regolith. *J. Geophys. Res.* **116**, E07004 (2011). doi:[10.1029/2011je003805](https://doi.org/10.1029/2011je003805)
- J.C. Santamarina, K.A. Klein, M.A. Fam, *Soils and Waves* (Wiley, New York, 2001)
- K. Seiferlin, P. Ehrenfreund, J. Garry, K. Gunderson, K. Hütter, G. Kargl, A. Maturilli, J.P. Merrison, Simulating Martian regolith in the laboratory. *Planet. Space Sci.* **56**, 2009–2025 (2008)
- T. Spohn et al., InSight: measuring the Martian heat flow using the heat flow and physical properties package (HP³), in *43rd Lunar Planetary Science, Abstract #1445* (Lunar and Planetary Institute, Houston, 2012)
- C. Vrettos, Shear strength investigations for a class of extra-terrestrial analogue soils. *J. Geotech. Geoenviron. Eng.* **138**, 508–515 (2012)